Hindawi
Advances in Materials Science and Engineering
Volume 2018, Article ID 3701682, 9 pages
https://doi.org/10.1155/2018/3701682

Research Article

Investigation of Microstructural Damage in Ultrahigh-Performance Concrete under Freezing-Thawing Action

Chunping Gu[1,2] **Wei Sun**[3] **Liping Guo**[3] **Qiannan Wang**[3] **Jintao Liu**[1,2] **Yang Yang**[1,2] **and Tao Shi**[1,2]

[1]*College of Civil Engineering and Architecture, Zhejiang University of Technology, Hangzhou 310023, China*
[2]*Key Laboratory of Civil Engineering Structures and Disaster Prevention and Mitigation Technology of Zhejiang Province, Zhejiang University of Technology, Hangzhou 310023, China*
[3]*School of Materials Science and Engineering, Southeast University, Nanjing 211189, China*

Correspondence should be addressed to Liping Guo; guoliping691@163.com

Received 9 January 2018; Revised 21 February 2018; Accepted 12 March 2018; Published 5 April 2018

Academic Editor: Antonio Gilson Barbosa de Lima

This work aims to investigate the damage in ultrahigh-performance concrete (UHPC) caused by freezing-thawing action. Freezing-thawing tests were carried out on UHPCs with and without steel fibers. Mercury intrusion porosimetry (MIP), scanning electron microscopy (SEM), and X-ray computed tomography (X-ray CT) were applied to detect the microstructure of the UHPC matrix before and after the freezing-thawing tests. The results showed that UHPC possessed very excellent freezing-thawing resistance due to its dense microstructure. After the freezing-thawing action, cracks occurred and were prone to initiate at the sand-paste interface in the UHPC matrix. MIP results also indicated that cracks appeared in the UHPC matrix after the freezing-thawing action. The number of defects that can be seen by X-ray CT increased in UHPC after the freezing-thawing action as well. The mismatch of the thermal expansion coefficients of the aggregate and the paste is considered to be the reason for the cracking at the sand-paste interface. The steel fibers in UHPC inhibited the propagation of cracks in the matrix and improved the freezing-thawing performance of UHPC.

1. Introduction

Ultrahigh-performance concrete (UHPC) is a novel type of cementitious material, which shows extremely excellent mechanical properties and durability [1, 2]. Due to its excellent performance, UHPC is considered to be a sustainable and economical material for various structures, such as hydraulic structures, thin-layer structures, marine structures, and military structures [3].

UHPC also can be used in some cold regions because of its great resistance to freezing-thawing damage [4, 5]. In cold regions, the freezing-thawing action is a very common cause for the deterioration of concrete structures. The damage process in normal concrete under freezing-thawing action has been widely studied, from the point of views of both microstructure and macroproperties [6–8]. Two types of damage, that is, surface scaling and internal cracking, would be induced when the concrete undergoes freezing-thawing cycles. In order to quantify these types of damage caused by freezing-thawing action, several methods have been developed. Normally, the surface scaling is evaluated by the mass loss, and the internal cracking is reflected by the change of relative dynamic modulus of elasticity [9, 10]. The internal cracks and pore structures in mortar or concrete damaged by freezing-thawing action also have been characterized by various techniques, such as mercury intrusion porosimetry (MIP) and scanning electron microscopy (SEM) [11–13]. These efforts were mostly made on concretes with a moderate strength, while the freezing-thawing microstructural damage in UHPC was rarely studied. Since UHPC is a promising material with wide potential applications, it is of significance to investigate the damage process of UHPC exposed to freezing-thawing action, especially from the microstructural point of view.

The aim of this paper is to investigate the freezing-thawing resistance of UHPC and to reveal the microstructure evolution of UHPC under the freezing-thawing action. It was anticipated that microstructural observations could improve the understanding of the deterioration mechanism of UHPC subjected to freezing-thawing action. In this paper, SEM was used to detect the cracks caused by freezing-thawing action in UHPC. MIP and X-ray computed tomography (X-ray CT) were applied to track the pore structure evolution of UHPC during the freezing-thawing action. Furthermore, based on the test results, the role of steel fibers in the freezing-thawing resistance of UHPC was also discussed in the paper.

2. Materials and Methods

2.1. Materials. UHPCs with and without steel fibers were prepared in the study. Type P•II 52.5R Portland cement, Class F fly ash (FA), and silica fume (SF) were used as cementitious materials. The chemical and physical properties of the cement, FA, and SF are shown in Table 1 [14]. The addition of FA could reduce the hydration heat and improve the workability of UHPC. The aggregates were river sand, whose particle size was smaller than 2.36 mm. The superplasticizer was a type of the liquid agent with a solid content of 28%. Copper-coated steel fibers were used to improve the ductility of UHPC, and the length and diameter of the fibers were 13 mm and 0.2 mm, respectively.

The proportions of UHPCs are shown in Table 2. All the UHPCs had the same matrix, while UHPC-1%, UHPC-2%, and UHPC-3% were reinforced with different amounts of steel fibers. In order to make the comparison more clearly, the proportion was given in a percentage form. Abbreviations are used in Table 2, that is, C = cement, B = binder, FA = fly ash, SF = silica fume, RS = river sand, Sup = superplasticizer, W = water, and V_f = volume fraction of steel fibers. The binder means the sum of the cement, FA, and SF. The cement usages of UHPCs were more or less the same, which were about 540 kg/m^3. The specimens were cast into 40 mm × 40 mm × 160 mm molds, and after demolding, they were cured in the standard condition (20°C, RH > 95%) for 90 days.

2.2. Mechanical Tests. Flexural and compressive tests were performed following the standard GB/T17671-1999 [15]. Firstly, the three-point bending test was performed to determine the flexural strength. Afterwards, two portions from each specimen broken in flexure were used for compressive tests. Three specimens of each batch were tested.

2.3. Freezing-Thawing Tests. The freezing-thawing tests were performed based on the standard GB/T50082-2009 [16]. The temperature range of a freezing-thawing cycle was −20°C~20°C, and one cycle lasts about 4 hours. After enduring a certain number of freezing-thawing cycles, the mass and relative dynamic modulus of elasticity of the specimens were measured. In the standard, 300 freezing-thawing cycles were recommended for testing the freezing-thawing performance of normal concrete. But UHPC normally does not degrade at 300 cycles. Hence, the number of freezing-thawing cycles was increased to 800 in this study.

Table 1: Chemical and physical properties of the cement, FA, and SF.

		Binder		
		Cement	Fly ash	Silica fume
Chemical composition (%)	SiO_2	20.40	54.88	94.48
	Al_2O_3	4.70	26.89	0.27
	Fe_2O_3	3.38	6.49	0.83
	CaO	64.70	4.77	0.54
	MgO	0.87	1.31	0.97
	SO_3	1.88	1.16	0.8
	K_2O	0.45	1.05	—
	Na_2O	0.38	0.88	—
	Loss	3.24	2.56	2.11
Physical properties	Specific density (kg/m^3)	3130	2240	2500
	Specific surface area (m^2/kg)	362	454	22000

Table 2: Mixture proportion of UHPCs.

	C/B	FA/B	SF/B	RS/B	Sup/B	W/B	V_f
Plain UHPC	0.5	0.4	0.1	1.2	3.5%	0.16	0%
UHPC-1%	0.5	0.4	0.1	1.2	3.5%	0.16	1%
UHPC-2%	0.5	0.4	0.1	1.2	3.5%	0.16	2%
UHPC-3%	0.5	0.4	0.1	1.2	3.5%	0.16	3%

2.4. SEM. A Sirion field emission scanning electron microscopy was used for the imaging of the cracks induced by the freezing-thawing action. After enduring 800 freezing-thawing cycles, the UHPC specimens were crashed, and small samples were chosen for the SEM tests. Secondary electron images were taken at the fractured surfaces.

2.5. MIP. The porosities and pore size distributions of UHPC specimens were detected with MIP. Crashed pieces of the matrix of UHPCs were served as samples. The samples were immersed in acetone for 7 days to stop the hydration. Then, they were oven-dried at 50°C for 3 days. The dried samples were used for the MIP tests, which were performed with Micromeritics AutoPore IV 9500. The contact angle was set to be 130°, and the detected pore sizes were between 3 nm and 360 μm.

2.6. X-Ray CT. X-ray CT was employed to detect the distribution of defects in UHPC. The YXLON microfocus X-ray CT system was used to scan the UHPC specimens before and after the freezing-thawing tests. The X-ray peak energy and current were 195 kV and 0.41 mA, respectively. The sample was a 40 mm × 40 mm × 160 mm prism, and the obtained voxel size was 64 μm × 64 μm × 64 μm.

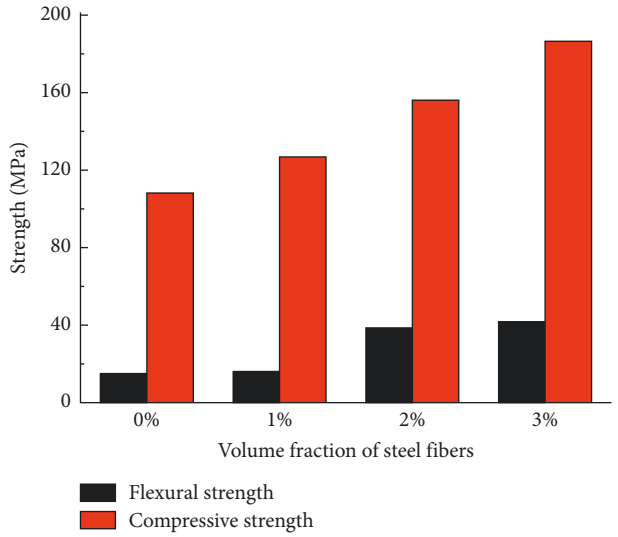

Figure 1: Compressive strength and flexural strength of UHPC specimens.

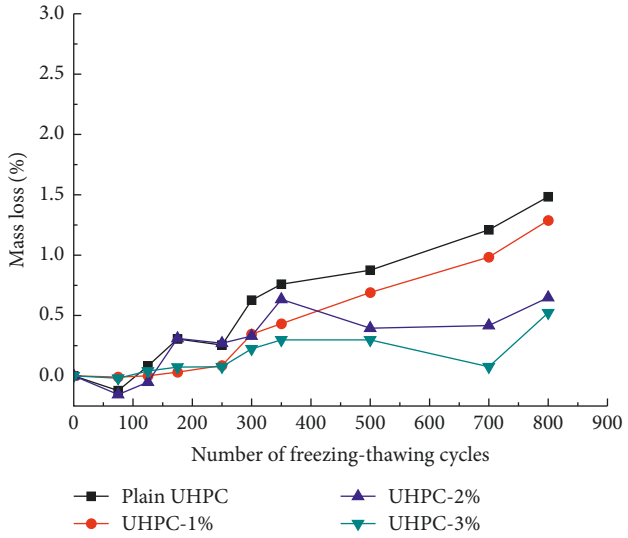

Figure 2: Mass loss of UHPCs at different freezing-thawing cycles.

3. Results and Discussion

3.1. Mechanical Properties of UHPC. Figure 1 shows the compressive strength and flexural strength of the UHPC specimens. The addition of steel fibers significantly increased the compressive and flexural strengths of UHPC. Compared to plain UHPC, the compressive and flexural strengths of UHPC-3% were improved by 72.4% and 178.7%, respectively. The strengthening effect of steel fibers in UHPC is much more significant than that in normal concrete [17] because of the strong bond between the fibers and matrix in UHPC.

3.2. Freezing-Thawing Performance of UHPC. The test results showed that UHPC exhibited great freezing-thawing resistance. Figure 2 demonstrates the mass loss of UHPC specimens during the freezing-thawing tests. The mass loss

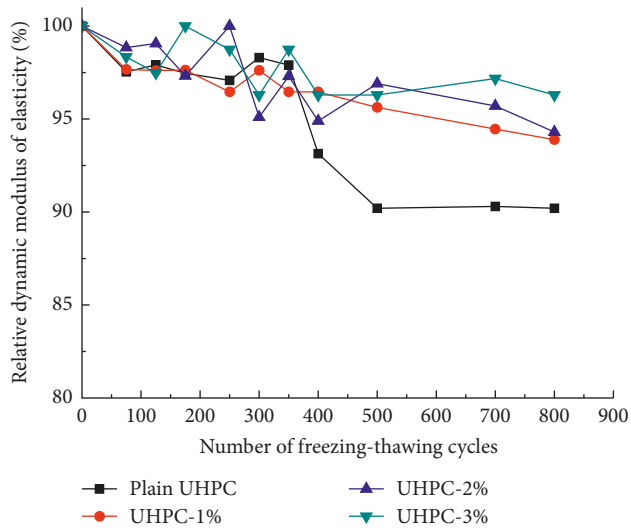

Figure 3: Relative dynamic modulus of elasticity of UHPCs at different freezing-thawing cycles.

of UHPC specimens increased slightly with the number of freezing-thawing cycles. After enduring 800 cycles, the mass losses of UHPC specimens were all less than 1.5%. The surface scaling was the main reason for the mass loss. Figure 3 shows the evolution of the relative dynamic modulus of elasticity of UHPC specimens at different freezing-thawing cycles. The relative dynamic modulus of elasticity of UHPC specimens was reduced very slightly with the increase of the cycles until it reached 350 cycles. It suggested that UHPCs did not show significant internal deterioration before that. After the freezing-thawing tests, the relative dynamic modulus of elasticity was approximately more than 90% for all UHPC specimens.

It can also be seen from Figures 2 and 3 that the presence of steel fibers could improve the freezing-thawing performance of UHPC. After going through 800 freezing-thawing cycles, UHPC with higher dosage of steel fibers exhibited lower mass loss and higher relative dynamic modulus of elasticity. The crack-bridging effect of steel fibers plays an importance role for the improvement of freezing-thawing resistance of UHPC.

The findings from other literatures also indicated that UHPC exhibited very excellent freezing-thawing resistance [18–21]. After enduring 300 freezing-thawing cycles, the relative dynamic modulus of elasticity of UHPCs normally did not decrease, and the mass losses were less than 0.5% [18, 19]. In order to clearly reveal the freezing-thawing performance of UHPC, more cycles were adopted in the freezing-thawing tests by several studies. After 600 freezing-thawing cycles, the relative dynamic modulus of elasticity and mass losses of UHPCs with different curing regimes did not obviously change [4, 20], which implied that the degradation in UHPC induced by freezing-thawing cycles was negligible. After 1000 freezing-thawing cycles, the relative dynamic modulus of elasticity of UHPC was 90%, and the compressive strength of UHPC reduced by 6% [21]. Generally, the UHPCs with heat curing have better freezing-thawing performance than standard-cured UHPCs [18, 20].

(a) (b)

Figure 4: Cracked UHPC specimens (40 mm × 40 mm × 160 mm) after enduring 250 freezing-thawing cycles: (a) plain UHPC and (b) UHPC-1%.

The hydration products in UHPC with heat curing were denser than those with standard curing; hence, the freezing-thawing performance of heat-cured UHPC was extremely excellent, and no obvious freezing-thawing damage could be observed. In this study, the standard curing were adopted, so the UHPCs degraded a little after 800 freezing-thawing cycles, and the test results were close to those in the literatures [21].

Besides the test results, an unexpected phenomenon was observed during the freezing-thawing experiments. One plain UHPC specimen and one UHPC-1% specimen were cracked severely after 250 freezing-thawing cycles, as seen in Figure 4. The crack pattern looked like being hit by an impact load. All the other specimens were in good condition, so the data for these two specimens were eliminated when calculating the mass loss and relative dynamic modulus of elasticity.

The reason for this phenomenon is still under investigation. The probable reason lies in the existence of big river sand particles (max. 2.36 mm) or large air pores in UHPC [22]. Both big river sand particles and large air pores could influence the homogeneity of UHPC and arouse stress concentration in UHPC, resulting in sudden severe cracking. The brittleness of the UHPC matrix also contributes to this phenomenon. Based on this finding, at least 2% of steel fibers is recommended to add in UHPC in order to ensure the safety of UHPC structures in cold regions.

3.3. Cracks in UHPC Induced by Freezing-Thawing Action. Before the freezing-thawing action, UHPC had a very dense microstructure. Capillary pores and $Ca(OH)_2$ crystals were hardly seen, and the interfacial transition zones (ITZs) almost disappeared in UHPCs. Figure 5 shows the bond between the sand and the paste in plain UHPC, and Figure 6 shows the bond between the fiber and the matrix in UHPC-2%. It was observed that both the sand-paste and fiber-matrix bonds were very intense, and ITZs were difficult to tell. The previous nanoindentation study proved that the micromechanical properties of the ITZ and the bulk paste of the UHPC were similar to each other [23], which indicated that the weak ITZ disappeared in UHPC. This is one of the reasons why UHPC possesses extremely excellent mechanical properties and resistance to aggressive agents.

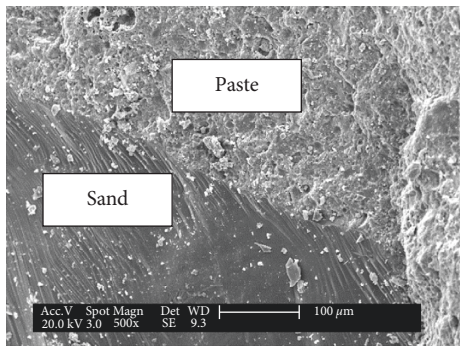

Figure 5: The bond between the sand and paste in plain UHPC.

In addition to the dense microstructure, spherical air voids also can be observed in UHPC as shown in Figure 7. This image was taken from a plain UHPC sample, and air

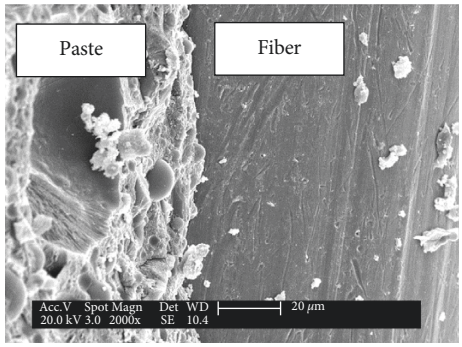

Figure 6: The bond between the fiber and the matrix in UHPC-2%.

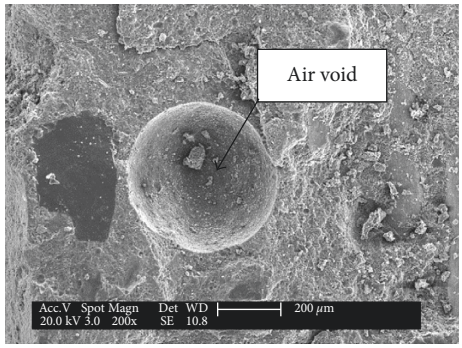

Figure 7: Air void in plain UHPC.

voids also existed in UHFC with steel fibers. The fresh UHPC mixture shows higher viscosity than normal concrete, so air bubbles are easily to be trapped in the UHPC mixture during casting. Researches have shown that the incorporation of air voids could improve the freezing-thawing resistance of normal concrete [13, 24].

After enduring 800 freezing-thawing cycles, microcracks can be found in plain UHPC. An example is given in Figure 8. The crack was initiated around the sand particle and went through an air void. Cracks at the ITZ between the fiber and matrix in UHPC with fibers were also detected with SEM. But it was difficult to determine whether the crack was caused by the freezing-thawing action or by sampling. The samples for SEM were prepared by crashing the UHPC specimen. The steel fiber might debond during crashing. For the plain UHPC sample, cracks mostly go through the fine aggregates (as shown in Figure 5) when undergoing mechanical load. Hence, the cracks around aggregates are more probably induced by freezing-thawing action.

3.4. Pore Structure Evolution of UHPC due to the Freezing-Thawing Action. The porosity and pore size distribution of plain UHPC and UHPC-2% matrices before and after the freezing-thawing tests were investigated with MIP. Before the freezing-thawing tests, the total porosities of plain UHPC and UHPC-2% matrix were 1.98% and 1.85%, respectively. After the tests, the total porosities of plain UHPC and UHPC-2% matrix increased to 6.05% and 3.32%, respectively. The increase in porosity due to freezing-thawing action was

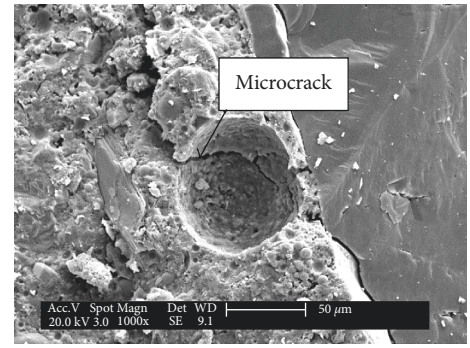

Figure 8: Microcracks in plain UHPC after the freezing-thawing tests.

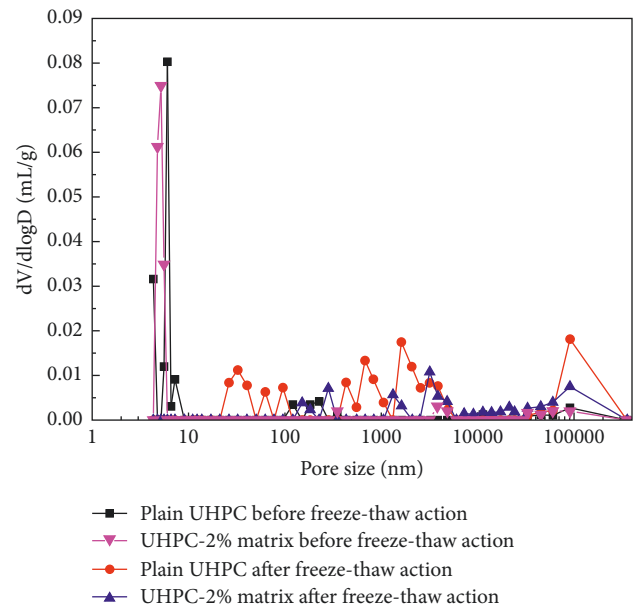

Figure 9: Pore size distribution of plain UHPC and UHPC-2% matrix before and after freezing-thawing tests.

reduced by steel fibers. Figure 9 shows the pore size distribution of plain UHPC and UHPC-2% before and after the freezing-thawing tests. It can be seen that, before the tests, most of the pores in plain UHPC and UHPC-2% matrix were gel pores, whose size was smaller than 10 nm. After being subjected to 800 freezing-thawing cycles, several new peaks appeared in the pore size distribution curve for both plain UHPC and UHPC-2% matrix. This implied that cracks were generated during the freezing-thawing tests. Compared with UHPC-2% matrix, more cracks existed in plain UHPC, which confirmed that the presence of steel fibers enhanced the freezing-thawing resistance of UHPC. It also can be seen from Figure 9 that, after the freezing-thawing tests, the peak for gel pores in the size distribution curve disappeared for both plain UHPC and UHPC-2% matrices. This may result from the ongoing hydration during the freezing-thawing tests. Water saturated condition was applied in the freezing-thawing tests, so UHPC could go on hydration and gel pores continued to be refined. Due to the limitation of the MIP test, it cannot detect pores smaller than 3 nm in this study.

It should be noted that the MIP only presents approximate results of the crack information in UHPC samples. As shown in Figure 8, cracks may go across the air voids, which would act as ink-bottle pores in the MIP test and influence the MIP results. In spite of this deviation, the MIP results still indicated that cracks existed in the freezing-thawing damaged UHPC samples.

3.5. Defects Evolution of UHPC due to the Freezing-Thawing Action. The 3D distribution of defects in UHPCs before and after the freezing-thawing tests was detected with X-ray CT. Figure 10 shows the distribution of defects in plain UHPC before the freezing-thawing tests. Because of the resolution limitation, the minimum volume of the defects was 0.002 mm^3. The defects were mostly the air voids in the specimen.

Due to the excellent freezing-thawing resistance of UHPC, the difference between the 3D defects distribution images of UHPC specimens before and after the freezing-thawing action was difficult to distinguish with naked eyes. Nevertheless, the data about the total defects volume and defects size distribution before and after the freezing-thawing action were still comparable. Table 3 shows the volume fraction of defects in UHPC specimens before and after freezing-thawing tests. The defects volume in UHPCs all increased after the freezing-thawing action. The increment for plain UHPC was 43.1%, while the increment for UHPC-3% was only 9.86%. Compared to UHPC-3%, more defects which can be detected with X-ray CT occurred in plain UHPC after the freezing-thawing action.

The defects volume distributions of UHPC specimens before and after freezing-thawing action were shown in Figure 11. The y-axis is the number of defects in a 40 mm × 40 mm × 160 mm UHPC specimen. It was noticed that most of the defects in UHPC were smaller than 0.1 mm^3. Before the freezing-thawing action, UHPC-3% had the largest amount of defects. This may be due to its relatively lower workability, which resulted from the addition of more steel fibers. After the freezing-thawing action, the number of defects all increased for the UHPC specimens. The defects with volume smaller than 0.1 mm^3 had the most significant increase. This was because that some smaller defects, which could not be detected by X-ray CT at first, became larger due to the freezing-thawing action. During the freezing-thawing action, cracks originated at the interface between the paste and aggregates and may go through the air pores, leading to the coalescing of two (or more) separated air voids. If the crack kept propagating, more air voids and cracks would be connected and form 3D crack networks. This phenomenon was observed in normal concrete [12]. Nevertheless, because of the presence of steel fibers and homogeneous microstructure, the crack propagation process in fiber-reinforced UHPC is much slower than that in normal concrete. As shown in Figure 11, the experimental results also proved that the defects in plain UHPC increased more than those in UHPC-3%. The presence of steel fibers improved the resistance of UHPC to freezing-thawing damage.

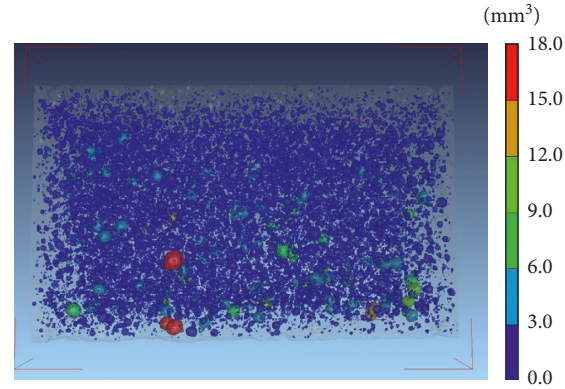

Figure 10: 3D defects distribution of a plain UHPC specimen (40 mm × 40 mm × 160 mm) before the freezing-thawing tests.

4. Discussions

According to the findings in this study, the presence of steel fibers improved the freezing-thawing performance of UHPC. Due to the low water-to-binder ratio and the pozzolanic reactivity of SF, the interfaces between the steel fibers and the matrix were very intense so that the fibers could bridge the cracks very efficiently. Hence, the crack propagation process could be inhibited if the fibers were presented, and more fibers would lead to higher cracking resistance. It is also the case for UHPC under freezing-thawing action. The microcracks induced by freezing-thawing cycles could be effectively bridged by the fibers so that the freezing-thawing performance of UHPC improved. On the other hand, if fibers were not present or not enough, UHPC might be damaged very suddenly (as shown in Figure 4) because of its high brittleness.

The hydraulic pressure and osmotic pressure are considered to be the main reasons for the deterioration of normal concrete subjected to freezing-thawing cycles [25]. When the stress aroused by these two kinds of pressure is higher than the tensile strength of concrete, cracking may occur. But these two pressures are both considered to originate from the icing of the water in the capillary pores of concrete. It is not the case for UHPC. It is well known that the freeze point of water in the porous material is related to the pore size, and it is estimated that water in gel pores does not freeze above −78°C [26]. For UHPC, large capillary pores are hardly seen [3, 27], and most of the pores in UHPC are gel pores. So when UHPC is subjected to freezing conditions, most of the water in gel pores will not turn into ice but continue to exist as liquid water. Therefore, the hydraulic pressure and osmotic pressure are not the main cause for the cracking in UHPC under freezing-thawing action.

According to the structural characteristics of UHPC, it may make more sense that the crack is resulted from the mismatch of the thermal expansion coefficients of the sand and paste. The thermal expansion coefficient of UHPC paste is between 15 and 20 $\mu m \cdot m^{-1} \cdot K^{-1}$ [28], while the thermal expansion coefficient of natural sand is around 10 $\mu m \cdot m^{-1} \cdot K^{-1}$ [26], which is much lower than that of

Table 3: Total volume fraction of defects in UHPC specimens before and after freezing-thawing tests.

	Plain UHPC	UHPC-1%	UHPC-2%	UHPC-3%
Before freezing-thawing tests	1.67%	2.12%	1.94%	2.84%
After freezing-thawing tests	2.39%	2.73%	2.56%	3.12%

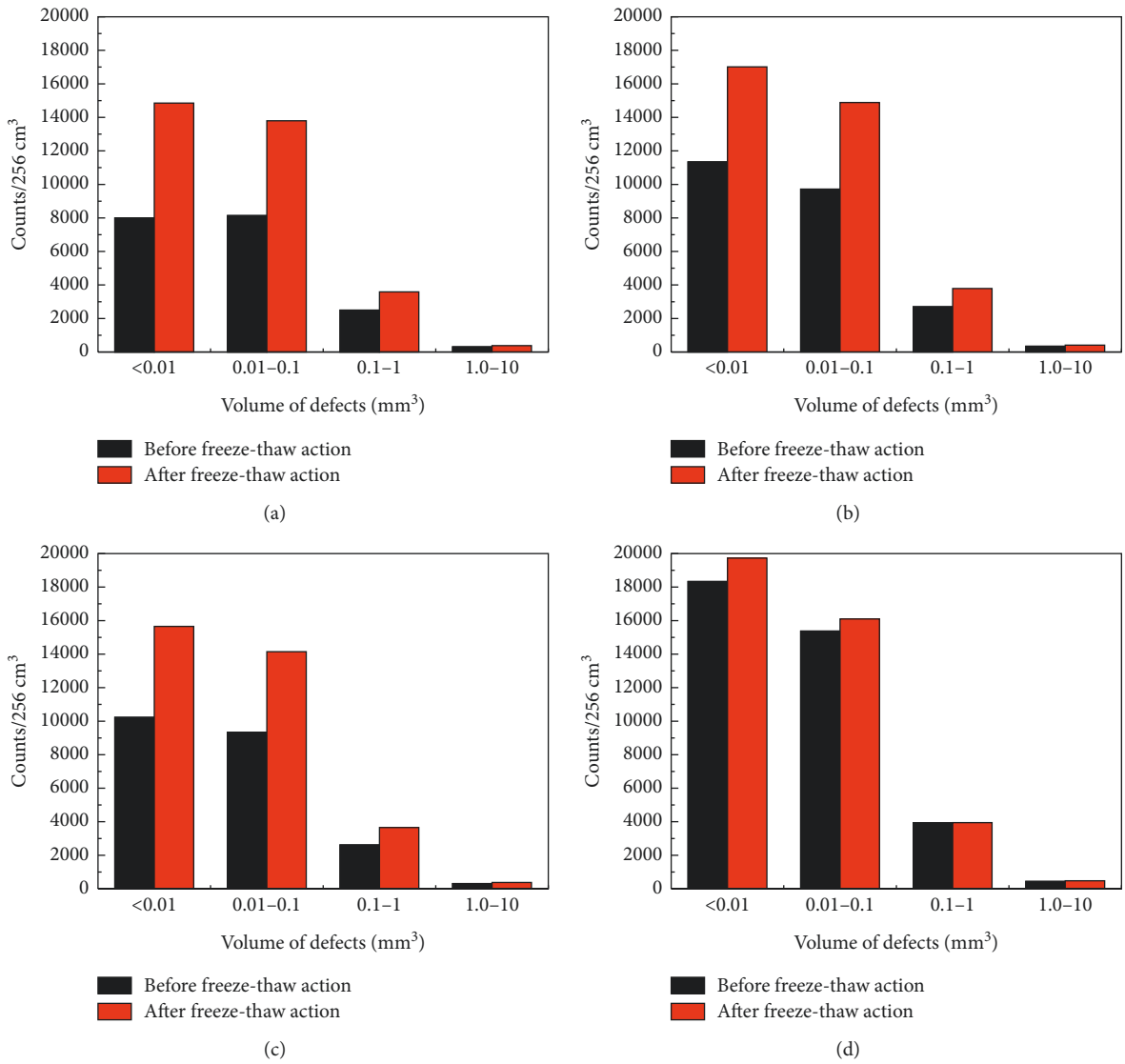

Figure 11: Defects volume distributions of UHPC specimens before and after freezing-thawing tests: (a) plain UHPC, (b) UHPC-1%, (c) UHPC-2%, and (d) UHPC-3%.

UHPC paste. The thermal expansion coefficients of the steel fiber and UHPC matrix are around 12 $\mu m \cdot m^{-1} \cdot K^{-1}$ and 11 $\mu m \cdot m^{-1} \cdot K^{-1}$, respectively [3]; hence, the stress aroused at the fiber-matrix interface is much lower than that at the sand-paste interface. Under the freezing-thawing action, the deformations of the sand and paste were different from each other, which aroused stress at the interface. It was more like a fatigue load at the interface of the aggregates and paste, when the temperature went up and down. Cracks initiated at the interface between the paste and aggregates, and may go through the air pores. When the freezing-thawing action is going on, cracks may connect to each other, and UHPC will fail in the end.

The approximate thermal expansion coefficients of commonly used aggregates were summarized as follows: 5 $\mu m \cdot m^{-1} \cdot K^{-1}$ for limestone; 6 $\mu m \cdot m^{-1} \cdot K^{-1}$ for basalt and gabbro; 7 $\mu m \cdot m^{-1} \cdot K^{-1}$ for granite; 9 $\mu m \cdot m^{-1} \cdot K^{-1}$ for dolerite; 10 $\mu m \cdot m^{-1} \cdot K^{-1}$ for sandstone and natural gravel; and 11 $\mu m \cdot m^{-1} \cdot K^{-1}$ for quartzite [26]. Hence, it is better to use sandstone, natural gravel, and quartzite as aggregates to prepare UHPC from the point of view of freezing-thawing performance. The use of limestone, basalt, and gabbro

should be avoided when preparing UHPCs that serve in cold regions.

5. Conclusions

This paper investigated the macroperformance and microstructure of UHPC before and after the freezing-thawing action. The following conclusions can be drawn:

(1) Compared to normal concrete, UHPC showed excellent freezing-thawing resistance, no matter steel fiber-reinforced or not. But unexpected cracking happened to one plain UHPC specimen and one UHPC-1% specimen. The reason of the cracking is worthy of further studying.

(2) Before the freezing-thawing action, UHPC had a very dense microstructure, but large amounts of air voids were trapped in UHPC. After going through 800 freezing-thawing cycles, cracks were induced in UHPC and prone to initiate at the ITZ between the aggregates and paste.

(3) The cracking in UHPC under freezing-thawing action may arise from the mismatch of the thermal expansion coefficients of the aggregates and paste. Sandstone, natural gravel, and quartzite were recommended to use as aggregates to prepare UHPC in cold regions. The presence of steel fibers could restrain the initiation and propagation of the cracks in UHPC, resulting in a great improvement of freezing-thawing resistance.

Conflicts of Interest

The authors declare that they have no conflicts of interest.

Acknowledgments

This work was supported by the National Basic Research Program of China (Grant no. 2015CB655102) and the China Postdoctoral Science Foundation-Funded Project (Grant no. 2017M612028), partly supported by the National Natural Science Foundation of China (Grant nos. 51708502, 51378113, and 51778583) and a Plan of Six Peak Talents in Jiangsu Province (Grant no. JZ-004).

References

[1] N. Roux, C. Andrade, and M. A. Sanjuan, "Experimental study of durability of reactive powder concretes," *Journal of Materials in Civil Engineering*, vol. 8, no. 1, pp. 1–6, 1996.

[2] J. Pierard, B. Dooms, and N. Cauberg, "Durability evaluation of different types of UHPC," in *Proceedings of the RILEM-fib-AFGC International Symposium on Ultra-High Performance Fiber-Reinforced Concrete*, pp. 275–284, Marseille, France, October 2013.

[3] C. Gu, G. Ye, and W. Sun, "Ultrahigh performance concrete-properties, applications and perspectives," *Science China Technological Sciences*, vol. 58, no. 4, pp. 587–599, 2015.

[4] B. Graybeal and J. Tanesi, "Durability of an ultrahigh-performance concrete," *Journal of Materials in Civil Engineering*, vol. 19, no. 10, pp. 848–854, 2007.

[5] M. Alkaysi, S. El-Tawil, Z. Liu, and W. Hansen, "Effects of silica powder and cement type on durability of ultra high performance concrete (UHPC)," *Cement and Concrete Composites*, vol. 66, pp. 47–56, 2015.

[6] H. Cai and X. Liu, "Freeze-thaw durability of concrete: ice formation process in pores," *Cement and Concrete Research*, vol. 28, no. 9, pp. 1281–1287, 1998.

[7] X. Ren, X. Wan, and T. Zhao, "Review of mechanism and mathematical model for salt scaling and freezing-thawing damage of concrete," *Concrete*, vol. 20, no. 9, pp. 15–18, 2012, in Chinese.

[8] L. Wang, Y. Cao, Z. Wang, and P. Du, "Evolution and characterization of damage of concrete under freeze-thaw cycles," *Journal of Wuhan University of Technology-Materials Science Edition*, vol. 28, no. 4, pp. 710–714, 2013.

[9] W. Sun, R. Mu, X. Luo, and C. Miao, "Effect of chloride salt, freeze-thaw cycling and externally applied load on the performance of the concrete," *Cement and Concrete Research*, vol. 32, no. 12, pp. 1859–1864, 2002.

[10] W. Sun, Y. Zhang, H. Yan, and R. Mu, "Damage and damage resistance of high strength concrete under the action of load and freeze-thaw cycles," *Cement and Concrete Research*, vol. 29, no. 9, pp. 1519–1523, 1999.

[11] S. Jacobsen, J. Marchand, and H. Hornain, "SEM observations of the microstructure of frost deteriorated and self-healed concretes," *Cement and Concrete Research*, vol. 25, no. 8, pp. 1781–1790, 1995.

[12] I. Vegas, J. Urreta, M. Frías, and R. García, "Freeze-thaw resistance of blended cements containing calcined paper sludge," *Construction and Building Materials*, vol. 23, no. 8, pp. 2862–2868, 2009.

[13] M. A. B. Promentilla and T. Sugiyama, "X-ray microtomography of mortars exposed to freezing-thawing action," *Journal of Advanced Concrete Technology*, vol. 8, no. 2, pp. 97–111, 2010.

[14] C. Gu, W. Sun, L. Guo, and Q. Wang, "Effect of curing conditions on the durability of ultra-high performance concrete under flexural load," *Journal of Wuhan University of Technology-Materials Science Edition*, vol. 31, no. 2, pp. 278–285, 2016.

[15] GB/T17671-1999, *Standard Test Method for Compressive Strength of Cement Mortar*.

[16] GB/T50082-2009, *Standard Test Method for Determining Long-Term Performance and Durability of Ordinary Concrete*.

[17] P. S. Song and S. Hwang, "Mechanical properties of high-strength steel fiber-reinforced concrete," *Construction and Building Materials*, vol. 18, no. 9, pp. 669–673, 2004.

[18] T. M. Ahlborn, D. L. Misson, E. J. Peuse, and C. G. Gilbertson, "Durability and strength characterization of ultra-high performance concrete under variable curing regimes," in *Proceedings of the 2nd International Symposium on Ultra High Performance Concrete*, pp. 197–204, Kassel, Germany, March 2008.

[19] W. Meng, M. Valipour, and K. H. Khayat, "Optimization and performance of cost-effective ultra-high performance concrete," *Materials and Structures*, vol. 50, no. 1, p. 29, 2017.

[20] S. Liu, W. Sun, W. Lin, and J. Lai, "Preparation and durability of a high performance concrete with natural ultra-fine particles," *Journal of the Chinese Ceramic Society*, vol. 11, pp. 1080–1085, 2003.

[21] M. G. Lee, Y. C. Wang, and C. T. Chiu, "A preliminary study of reactive powder concrete as a new repair material," *Construction and Building Materials*, vol. 21, no. 1, pp. 182–189, 2007.

[22] C. Gu, W. Sun, L. Guo, and J. Zong, "X-ray computer tomography studies of meso-defects evolution of UHPCC due to freezing-thawing action," in *Proceedings of the International Conference on Microstructural-Related Durability of Cementitious Composites*, pp. 317–323, Amsterdam, The Netherlands, April 2012.

[23] S. Zhao and W. Sun, "Nano-mechanical behavior of a green ultra-high performance concrete," *Construction and Building Materials*, vol. 63, pp. 150–160, 2014.

[24] N. P. Mayercsik, M. Vandamme, and K. E. Kurtis, "Assessing the efficiency of entrained air voids for freeze-thaw durability through modeling," *Cement and Concrete Research*, vol. 88, pp. 43–59, 2016.

[25] D. Niu, L. Jiang, M. Bai, and Y. Miao, "Study of the performance of steel fiber reinforced concrete to water and salt freezing condition," *Materials and Design*, vol. 44, pp. 267–273, 2012.

[26] P. K. Mehta and P. J. Monteiro, *Concrete: Microstructure, Properties and Materials*, McGraw-Hill, New York, NY, USA, 3rd edition, 2006.

[27] D. Wang, C. Shi, Z. Wu, J. Xiao, Z. Huang, and Z. Fang, "A review on ultra high performance concrete: part II. Hydration, microstructure and properties," *Construction and Building Materials,* vol. 96, pp. 368–377, 2015.

[28] I. Maruyama and A. Teramoto, "Temperature dependence of autogenous shrinkage of silica fume cement pastes with a very low water-binder ratio," *Cement and Concrete Research*, vol. 50, pp. 41–50, 2013.